The Astrophysical Journal, 607:1024–1031, 2004 June 1

ELECTROSTATIC DECAY OF BEAM-GENERATED PLASMA TURBULENCE

Alberto M. Vásquez[1] and Daniel O. Gómez[1]
Instituto de Astronomía y Física del Espacio, Casilla de Correos 67, Succursale 28, 1428 Buenos Aires, Argentina; albert@iafe.uba.ar
Received 2003 September 29; accepted 2003 December 9

ABSTRACT

The study of the evolution of a suprathermal electron beam traveling through a background plasma is relevant to the physics of solar flares and their associated type III solar radio bursts. As they evolve, guided by the coronal magnetic field lines, these beams generate Langmuir turbulence. The beam-generated turbulence is in turn responsible for the emission of radio photons at the second harmonic of the local plasma frequency, which are observed during type III solar radio bursts. To generate the radio emission, the beam-aligned Langmuir waves must coalesce, and therefore, a process capable of redirecting the turbulence in an effective fashion is required. Different theoretical models identify the electrostatic (ES) decay process $L_1 \rightarrow L_2 + S$ (where L indicates a Langmuir wave and S an ion-acoustic wave) as the redirecting mechanism for the L waves. Two different regimes have been proposed to play a key role: backscattering and diffusive (small-angle) scattering. This paper is a comparative analysis of the ES decay rate for each regime and of the different observable characteristics that are expected for the resulting ion-acoustic waves.

Subject headings: Sun: corona — Sun: radio radiation — turbulence

1. INTRODUCTION

During solar flares, large amounts of energy are released and transformed into coronal heating and particle acceleration, where regions of magnetic reconnection are believed to be the acceleration sites for suprathermal electron beams. Once accelerated, these beams travel through the coronal plasma guided by the coronal magnetic field lines, generating a variety of observable emissions. One long-standing discrepancy in the modeling of this phenomenon is that a beam with a given energy flux seems not to be able to simultaneously reproduce the observed emissivities in hard X-ray (HXR; due to nonthermal bremsstrahlung at the chromosphere) and radio emission (due to beam-generated Langmuir turbulence in the corona). Once the beam energy flux is set to reproduce the HXR levels, the derived radio emissivities tend to be much higher than observed levels (Emslie & Smith 1984; Hamilton & Petrosian 1987).

In this context, we have developed a model for the evolution of electron beams and the generation of Langmuir turbulence, and we have also computed the emission of radio waves due to the coalescence of the beam-excited Langmuir waves. Our models describe the evolution of the beam and the produced Langmuir turbulence, consistently considering the effect of both collisions and quasi-linear wave-particle interaction. The level of turbulence derived from our models is up to 2 orders of magnitude lower than in previous attempts (Vásquez & Gómez 1997). The production of photons at the second harmonic of the plasma frequency (radio waves) is the result of the coalescence of two Langmuir waves. In our model we *assume* that the beam-generated Langmuir waves become isotropic in an effective way, because of electrostatic (ES) decay $L_1 + L_2 \rightarrow T(2\omega_{pe})$. We find that an adequate treatment of the second-harmonic photon generation (relaxing the head-on approximation) yields further reductions of the radio emission (Vásquez, Gómez, & Ferro Fontán 2002). Although these results help to reduce the gap between the predicted HXR and radio emissivities, we find that further reductions are required.

The observed radio emission requires the coalescence of the beam-generated Langmuir waves. Therefore, a process capable of redirecting the turbulence in an effective fashion is required. Different models in the literature resort to ES decay $L_1 \rightarrow L_2 + S$ (where L indicates a Langmuir wave and S an ion-acoustic wave) as the redirecting mechanism for the L waves. Two different regimes have been proposed to play a key role. One of them is the so-called backscattering limit of the ES decay (Edney & Robinson 2001; Cairns 1987). In this limit, the primary Langmuir wave decays into another one that propagates in almost the opposite direction. The other asymptotic regime is the small-angle limit of the ES decay, which has also been pointed out by some authors as potentially relevant in this context (Melrose 1982; Tsytovich 1970). In this limit, the propagation directions of both Langmuir waves (L_1 and L_2) form a small angle, and the ES decay acts on the beam-generated Langmuir waves as a diffusion mechanism through $\boldsymbol{k}$-space. In our models described above, the isotropization of Langmuir waves has been an assumption rather than a result obtained from our beam-turbulence quasi-linear equations. If the timescale of the ES decay is short enough (as compared to the timescale for the Langmuir waves to escape their generation region), it is reasonable to expect that the small-angle limit will render the beam-generated Langmuir turbulence isotropic.

In this work we revise this approximation in detail. We compare the rate of ion-acoustic wave generation in both limits, for a given set of beam-generated Langmuir spectra. We also analyze the resulting frequencies of the ion-acoustic waves produced in each limit and compare them against reported in situ observations.

In situ observations of type III solar radio bursts have shown clear evidence in support of the occurrence of ES decay simultaneous with Langmuir waves. For example, Cairns & Robinson (1995) have analyzed *ISEE 3* data that show the coexistence of high- and low-frequency ES waves, identified

[1] Also at the Department of Physics, University of Buenos Aires, Argentina.

as Langmuir and ion-acoustic waves, respectively, during a type III radio event. They analyze the observed low-frequency waves and find that their frequencies are consistent with those predicted by assuming ES decay acting in the backscattering limit. Similar observational works by Thejappa et al. (2003) and Thejappa & MacDowall (1998), analyzing *Ulysses* Unified Radio and Plasma Wave Experiment (URAP) data, also support the occurrence of ES decay in association with impulsive Langmuir waves excited during type III radio events. In the present paper we make an analysis similar to the one by Cairns & Robinson (1995) and find out that the URAP data analyzed by Thejappa & MacDowall (1998) and Thejappa et al. (2003) are consistent with ES decay acting in the diffusive limit.

This paper is organized as follows: In § 2 we revisit the ES decay and the general expression of its rate of occurrence. In § 3 we apply the general results to the specific case of a beam-generated Langmuir spectrum. We make a quantitative comparison between the diffusive and backscattering cases. In § 4 we compute the expected frequencies for the generated ion-acoustic waves for the particular type III solar radio bursts observed and studied by Thejappa & MacDowall (1998) and Thejappa et al. (2003). Finally, in § 5 we list our main conclusions.

2. ELECTROSTATIC DECAY RATE

The ES decay $L_1 \rightarrow L_2 + S$ must obey momentum and energy conservation, so that the wavevectors and frequencies satisfy

$$\boldsymbol{k}_{L_1} = \boldsymbol{k}_{L_2} + \boldsymbol{k}_S, \quad \Omega_{L_1} = \Omega_{L_2} + \Omega_S, \tag{1}$$

where the dispersion relationships are

$$\Omega_L(\boldsymbol{k}_L) \approx \omega_{\rm pe}\left[1 + \frac{3}{2}(k_L\lambda_{\rm De})^2\right],$$
$$\Omega_S(\boldsymbol{k}_S) \approx k_S V_S. \tag{2}$$

From these relations, we obtain the modulus and direction of the wavevectors of the resulting waves L_2 and S (see Fig. 1) with respect to the wavevector of the initial Langmuir wave L_1:

$$\cos(\alpha) \equiv \frac{\boldsymbol{k}_{L_1}\cdot\boldsymbol{k}_{L_2}}{k_{L_1}k_{L_2}} = \frac{k_{L_1} - \mu k_S}{k_{L_2}}, \tag{3}$$

$$\mu \equiv \cos(\beta) = \frac{\boldsymbol{k}_{L_1}\cdot\boldsymbol{k}_S}{k_{L_1}k_S} = \frac{k_S + 2k_0}{2k_L}, \tag{4}$$

$$k_0 \equiv \frac{1}{3}\frac{\omega_e}{V_{\rm Te}}\sqrt{\frac{m_e}{m_i}},$$
$$k_{L_2}^2 = k_{L_1}^2 - 2k_0 k_S. \tag{5}$$

The spectral density $N_{\boldsymbol{k}}^{\sigma}$ of the plasmons of type σ (with $\sigma = L$ and S in this case) is defined such that the volumetric density of plasmons is $n^{\sigma} = \int [d\boldsymbol{k}/(2\pi)^3] N_{\boldsymbol{k}}^{\sigma}$. In terms of these spectral densities, the rate of production of ion-acoustic (S) waves is (Tsytovich 1970)

$$\frac{dN_{\boldsymbol{k}_S}^S}{dt} = \int \frac{d\boldsymbol{k}_{L_1}\, d\boldsymbol{k}_{L_2}}{(2\pi)^6} w_L^{SL} \times \left[N_{\boldsymbol{k}_{L_1}}^L N_{\boldsymbol{k}_S}^S + N_{\boldsymbol{k}_{L_1}}^L N_{\boldsymbol{k}_{L_2}}^L - N_{\boldsymbol{k}_{L_2}}^L N_{\boldsymbol{k}_S}^S\right], \tag{6}$$

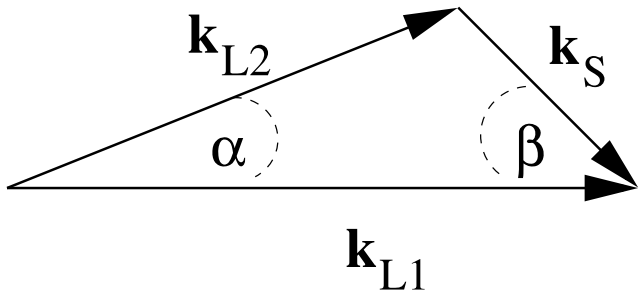

FIG. 1.—Momentum conservation in the ES decay, $\boldsymbol{k}_{L_1} = \boldsymbol{k}_{L_2} + \boldsymbol{k}_S$. Angles α and β are given by eqs. (4) and (5).

where the probability of the decay is

$$w_L^{SL} = \frac{\hbar e^2 \Omega_S^3 m_p (2\pi)^6}{8\pi m_e^3 V_{\rm Te}^4 k_S^2}\left(\frac{\boldsymbol{k}_{L_1}\cdot\boldsymbol{k}_{L_2}}{k_{L_1}k_{L_2}}\right)^2 \delta(\boldsymbol{k}_{L_1} - \boldsymbol{k}_{L_2} - \boldsymbol{k}_S) \times \delta(\Omega_{L_1} - \Omega_{L_2} - \Omega_S), \tag{7}$$

m_e and m_p are the electron and proton mass, respectively, $V_{\rm Te}$ is the electron thermal velocity, and the delta functions express the momentum and energy conservation.

3. RESULTS FOR BEAM-GENERATED LANGMUIR WAVES

We use the expressions of § 2 to compute the decay rate of a beam-generated Langmuir spectrum. Hereafter, we adopt a given shape for a beam-generated Langmuir spectrum. The dependence of the spectrum on the modulus of the wavenumber has been obtained by Vásquez & Gómez (1997). We also assume this spectrum to be axisymmetric and with a Gaussian angular spread about the direction of the beam, and we analyze the *initial* ES decay rates.

The beam-generated Langmuir turbulence is initially aligned with the beam propagation axis (the local magnetic field). As it proceeds, we expect the ES decay to redirect the Langmuir waves. We thus divide our analysis into two parts. In the first part we analyze the ES decay of a perfectly collimated Langmuir spectrum. Second, we analyze the same rates for a noncollimated spectrum. In both stages of our analysis, we compute and compare the rates for both the diffusive and backscattering cases.

3.1. *Collimated Langmuir Spectra*

Let us evaluate the initial rate of production of S waves generated by a Langmuir spectrum, which is in turn produced by a perfectly collimated beam (i.e., we take $N_{\boldsymbol{k}_{L_2}}^L = 0$):

$$\frac{1}{\tau(\boldsymbol{k}_S)} \equiv \frac{1}{N_{\boldsymbol{k}_S}^S}\frac{dN_{\boldsymbol{k}_S}^S}{dt} \approx \int \frac{d\boldsymbol{k}_{L_1}\, d\boldsymbol{k}_{L_2}}{(2\pi)^6} w_L^{SL} N_{\boldsymbol{k}_{L_1}}^L = \frac{K(T_e,\, n_e)}{(2\pi)^3}\int \frac{d\boldsymbol{k}_{L_1}}{(2\pi)^3}\frac{[\boldsymbol{k}_{L_1}\cdot(\boldsymbol{k}_{L_1} - \boldsymbol{k}_S)]^2}{k_{L_1}^2(\boldsymbol{k}_{L_1} - \boldsymbol{k}_S)^2} \times N_{\boldsymbol{k}_{L_1}}^L \delta\left(k_1\mu - \frac{k_s + 2k_0}{2}\right), \tag{8}$$

where the integral in $\boldsymbol{k}_{L_2}$ has been performed using momentum conservation and the function K is given by

$$K(T_e,\, n_e) = \frac{\hbar e^2 \Omega_S^3 m_i (2\pi)^6}{8\pi m_e^3 V_{\rm Te}^4 k_S^2}\frac{\omega_{\rm pe}}{3k_S V_{\rm Te}^2}. \tag{9}$$

In a previous work (Vásquez & Gómez 1997; Vásquez et al. 2002) we developed a model to derive the spectrum of beam-generated Langmuir waves. According to this model, the wavenumbers of the excited Langmuir waves lie in the range

$$k_1 = [k_{\min},\ k_{\max}] \approx [6,\ 12]k_0\sqrt{T_6}, \tag{10}$$

where $T_6 \equiv T_e/10^6$ K. Approximating the plasmon spectral density as constant within the wavenumber range given by equation (10), and calling e_Z the direction of the beam, for a perfectly collimated spectrum, we have

$$N^L_{\boldsymbol{k}_{L_1}} = (2\pi)^3 \frac{n^L}{\Delta k^L}\delta(k_{1x})\delta(k_{1y}), \tag{11}$$

where Δk^L is the spectral width, and the result for the initial production rate of ion-acoustic waves is

$$\frac{1}{\tau(\boldsymbol{k}_S)} = \frac{1}{\tau_0}P(k_S,\ \mu), \quad \frac{1}{\tau_0} \equiv \frac{\pi}{4}\frac{k_0}{\Delta k^L}\frac{\omega_{\rm pe}W^L}{n_e m_e V^2_{\rm Te}}, \tag{12}$$

where the dimensionless function $P(k_S,\ \mu)$ is given by

$$P(k_S,\ \mu) \equiv \frac{1}{\mu}\frac{[2 + (k_S/k_0)(1-2\mu^2)]^2}{4 + (k_S/k_0)^2 + 4(k_S/k_0)(1-2\mu^2)} \quad \text{if } 6\sqrt{T_6} < \frac{k + 2k_0}{2\mu} < 12\sqrt{T_6} \tag{13}$$

and is zero otherwise. Figure 2 shows the dimensionless decay rate $P(k_S,\ \mu)$ given by equation (13) as a function of the wavenumber k_S and the angle θ_{SL} between $\boldsymbol{k}_S$ and $\boldsymbol{k}_L$. Here we have taken $T_6 = 0.17$ as a characteristic number for the type III solar radio burst analyzed in § 4. This graphic confirms that the cases of maximum probability of occurrence are backscattering (with $\theta_{SL} \to 0$, $P \sim 1$) and diffusive scattering (with $\theta_{SL} \sim 75^\circ$, $P \sim 4$). The factor of 4 in the diffusive decay rate results from the modulation factor $1/\mu$ in equation (13).

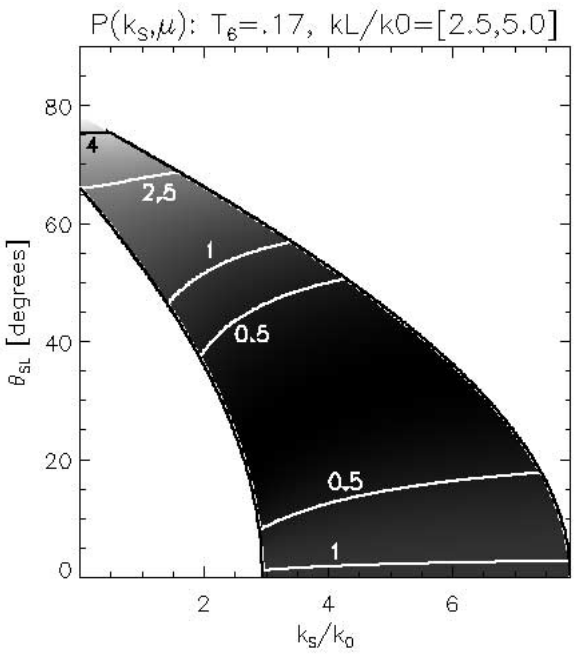

FIG. 2.—Dimensionless decay rate $P(\boldsymbol{k}_S)$ as a function of $(k_S,\ \theta_{SL})$, where $T_6 = 0.17$ and k_L/k_0 is in the range 2.5–5.0.

The propagation direction of the resulting ion-acoustic wave is parallel to the beam propagation in the case of backscattering and almost perpendicular to the beam in the diffusive case (with $k_S \ll k_L$). We therefore find that the decay rate becomes maximum for two limiting cases: (1) small-angle (diffusive) scattering, $\alpha \to 0$, and (2) backscattering, $\alpha \to \pi$.

Under the diffusive scattering approximation, estimates for the characteristic isotropization and energy transfer timescales indicate that the latter is much larger, implying that the isotropization occurs in a quasi-elastic fashion (Tsytovich 1970; see also Vásquez et al. 2002). The quasiconservation of the total energy is readily seen from the following argument: The ES decay conserves the total number of Langmuir plasmons. Now, given the weak dependence of their energy on the wavenumber (see eq. [2]), we can approximate the energy of each plasmon as $\omega_{\rm pe}$. Therefore, this decay cannot produce a significant change in the total Langmuir wave energy.

3.2. *Noncollimated Langmuir Spectra*

In § 3.1 we found that the ES decay of the one-dimensional Langmuir spectrum generated by a perfectly collimated beam is initially dominated by small-angle decay processes and, in the second place, by backscattering. We therefore expect that after a transient stage, the Langmuir spectrum will no longer be perfectly aligned with the beam direction, and also that a growing backscattered spectrum will arise. Nonetheless, we expect that the forward spectrum will contain much more energy than the backward spectrum, at least during the early stages of the evolution. Under this assumption, we consider now an axisymmetric spectrum around the beam direction and model it through functions $N_{\boldsymbol{k}} = N(\theta,\ k)$ that peak in the forward direction and monotonically decrease as $\theta \to \pi$.

Let us start by analyzing the small-angle scattering limit, i.e., $k_S \ll k_L$. For the diffusive decay, we have that the spectral width of the ion-acoustic waves produced is much smaller than the spectral width of the primary Langmuir waves. More specifically, we have

$$\frac{\Delta k_S}{\Delta k_L} \sim 3\frac{\langle k_S\rangle}{\langle k_L\rangle} \ll 1, \tag{14}$$

where $\langle k_S\rangle = k_{S,\,\max}/2$ and $\langle k_L\rangle = (k_{\min} + k_{\max})/2$ indicate mean wavenumber values. As the decay proceeds, each ES decay process will produce one ion-acoustic wave; hence,

$$N^L\Delta k_L \sim N^S\Delta k_S \to \frac{N^L}{N^S} \sim \frac{\Delta k_S}{\Delta k_L} \ll 1, \tag{15}$$

i.e., the *spectral* density of the (emitting) Langmuir waves becomes much lower than that of the (emitted) ion-acoustic waves (even though the Langmuir energy density can be much larger than that of the ion-acoustic waves). Thus, we neglect the term N^LN^L in the decay rate given by equation (6) and approximate

$$\begin{aligned}\frac{1}{\tau(\boldsymbol{k}_S)} &\equiv \frac{1}{N^S_{\boldsymbol{k}_S}}\frac{dN^S_{\boldsymbol{k}_S}}{dt} \approx \int \frac{d\boldsymbol{k}_{L_1}\,d\boldsymbol{k}_{L_2}}{(2\pi)^6} w^{SL}_L\left(N^L_{\boldsymbol{k}_{L_1}} - N^L_{\boldsymbol{k}_{L_2}}\right)\\ &= \frac{K}{(2\pi)^6}\int d\boldsymbol{k}_{L_1}\,\frac{\cos^2(\alpha)}{\mu}\left(N^L_{\boldsymbol{k}_{L_1}} - N^L_{\boldsymbol{k}_{L_2}}\right)\\ &\quad\times\delta\left(k_{L_1} - \frac{2k_0 + k_S}{2\mu}\right),\end{aligned} \tag{16}$$

where K is given by equation (9) (see also eq. [8]). Using energy conservation, equation (16) reduces to the double integral

$$\frac{1}{\tau(\boldsymbol{k}_S)} \approx \frac{K}{(2\pi)^6} \int_0^{2\pi} d\phi_1 \int_0^{\pi} d\theta_1 \, \sin\theta_1 \left\{ \frac{k_1^2 \cos^2(\alpha)}{\mu} \times [N(k_1, \theta_1) - N(k_2, \theta_2)] \right\}_{k_1=(k_S+2k_0)/(2\mu)}, \quad (17)$$

where we have assumed that the Langmuir spectrum $N_{\boldsymbol{k}}$ is symmetric about the beam propagation axis $\boldsymbol{e}_Z$ (i.e., independent of the angle ϕ), the values k_2 and θ_2 are related to k_1 and θ_1 through

$$k_2 = \sqrt{k_1^2 - 2k_0 k_1}, \quad (18)$$

$$\cos(\theta_2) = \frac{(\boldsymbol{k}_{L_1} - \boldsymbol{k}_S) \cdot \boldsymbol{e}_Z}{k_2}, \quad (19)$$

and $\cos(\alpha)$ is given by equation (3). We note here that in the backscattering limit, the term $N_{L_1} N_{L_2}$ cannot be neglected. Instead, for backscattering, we expect that $N_{L_2} \ll N_{L_1}$ (at early stages of the evolution), and hence, we can neglect the last two terms in equation (6). Therefore, the rate for backscattering can be obtained from equation (17) simply by neglecting the second term N_{θ_2} and also taking the limits $\cos(\alpha) \to -1$ and $\mu \to +1$.

To compare these rates against the perfectly collimated case (eq. [12]), let us multiply and divide the right-hand side of equation (17) by $K_1 \equiv (2\pi)^3 n_L / \Delta k_L$, to obtain

$$\frac{1}{\tau(\boldsymbol{k}_S)} = \frac{1}{\tau_0} P_1(k_S, \theta_S), \quad (20)$$

where $1/\tau_0$ is the reference rate given by equation (12), θ_S is the angle between the ion-acoustic wavevector and the beam propagation direction $\boldsymbol{e}_Z$, and the dimensionless function $P_1(k_S, \theta_S)$ is given by

$$P_1(k_S, \theta_S) = \frac{\Delta k_L}{n_L} \frac{1}{(2\pi)^3} \int_0^{2\pi} d\phi_1 \int_0^{\pi} d\theta_1 \, \sin\theta \left\{ \frac{k_1^2 \cos^2(\alpha)}{\mu} \times [N(k_1, \theta_1) - N(k_2, \theta_2)] \right\}_{k_1=(k_S+2k_0)/(2\mu)}. \quad (21)$$

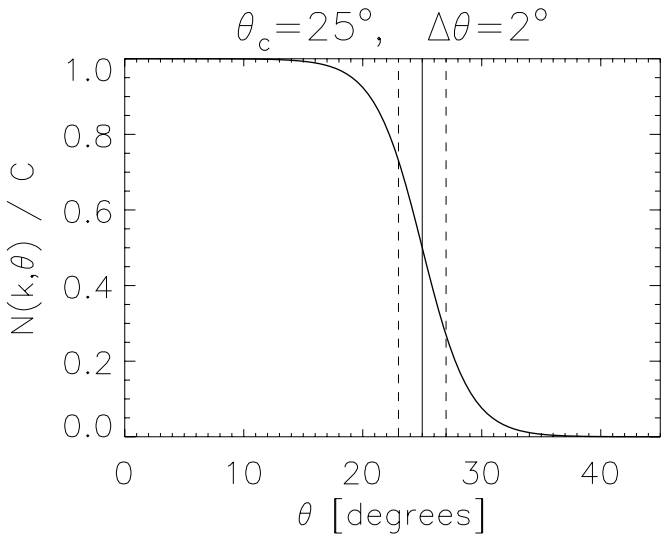

FIG. 3.—Model for the angular distribution of the Langmuir spectrum, with $\theta_c = 25^\circ$ and $\Delta\theta = 2^\circ$. The vertical lines indicate the angles θ_c (*solid line*) and $\theta_c \pm \Delta\theta$ (*dashed lines*).

We use this expression to evaluate the decay rate for a spectral model that is stronger in the forward direction (but not collimated). Here we neglect the dependence on wavenumber and assume the spectral density as constant within the range $[k_{\min}, k_{\max}]$ given by equation (10). More specifically, we consider

$$N(k, \theta) = C \frac{1 + e^{-\theta_c/\Delta\theta}}{1 + e^{(\theta-\theta_c)/\Delta\theta}} \text{ if } k_{\min} < k < k_{\max}, \quad (22)$$

where the normalization constant C is such that the number density of Langmuir plasmons is $n^L = \int [d\boldsymbol{k}/(2\pi)^3] N_{\boldsymbol{k}}$. As an example, Figure 3 shows this function for $\theta_c = 25^\circ$, $\Delta\theta = 2^\circ$. This angular distribution peaks at $\theta = 0$ and monotonically decreases with increasing θ. The mean value is reached at θ_c. Thus, for smaller values of this parameter, the spectrum is more collimated. The parameter $\Delta\theta$ measures the half-width over which the function varies from 75% to 25% of its

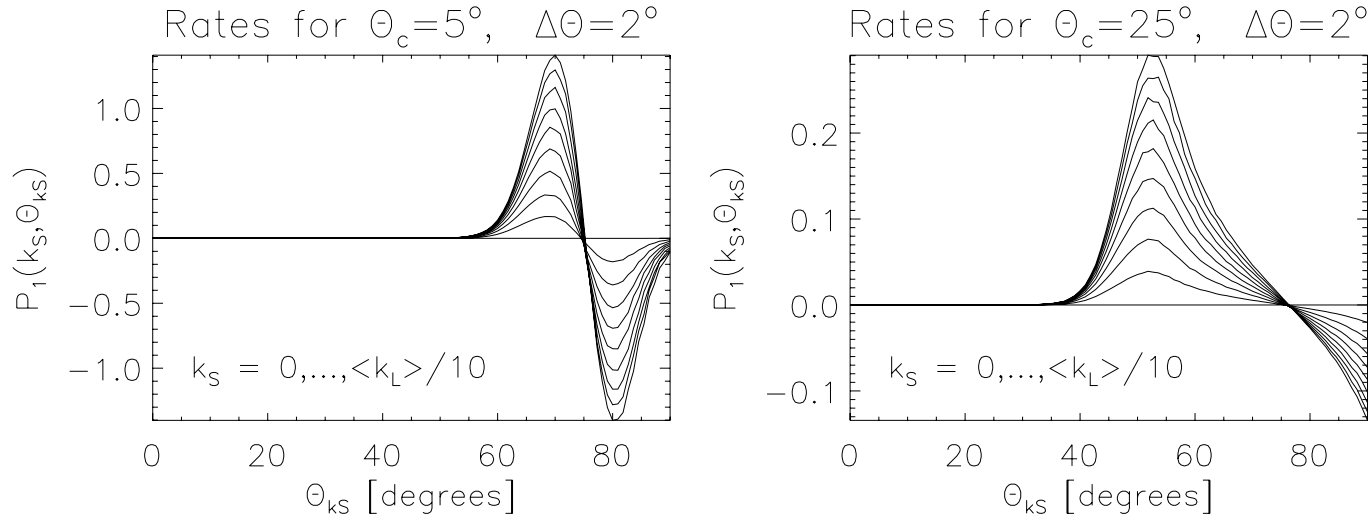

FIG. 4.—Dimensionless factor $P_1(k_s, \theta_S)$ for diffusive decay, with $\theta_c = 5^\circ$ (*left*) and 25° (*right*) and $\Delta\theta = 2^\circ$ in both panels. Profiles are plotted as a function of θ_S, with different curves corresponding to $k_S = 0, \ldots, \langle k_L \rangle/10$ (curves with larger P_1 values correspond to larger k_S).

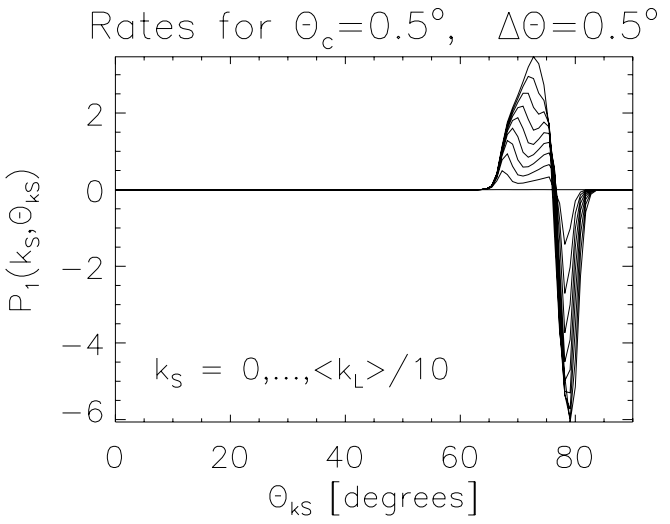

FIG. 5.—Dimensionless factor $P_1(k_s,\ \theta_S)$ for diffusive decay, with $\theta_c = 0.^\circ 5$ and $\Delta\theta = 0.^\circ 5$. Profiles are plotted as a function of θ_S, with different curves corresponding to $k_S = 0, \ldots, \langle k_L\rangle/10$ (curves with larger P_1 values correspond to larger k_S).

maximum value. For smaller values of this parameter, the spectrum has a sharper angular edge.

Figure 4 shows the resulting P_1 for two sharp-edged angular spectra with $\Delta\theta = 2^\circ$. One spectrum is well concentrated along the beam direction with $\theta_c = 5^\circ$, and the other corresponds to a wider distribution with $\theta_c = 25^\circ$. Our expression for P_1 (eq. [21]) is valid in the diffusive regime $k_S \ll k_L$, so we show results for $k_S = 0, \ldots, \langle k_L\rangle/10$. Rates monotonically increase with k_S, until they saturate at about $\langle k_L\rangle/5$. For larger values of k_S, the rates decrease with increasing k_S.

Higher rates are obtained for a more collimated beam, and the peak value is reached at a larger angle θ_S. This behavior can be understood in terms of our analytic decay analysis for the perfectly collimated case. The peak is expected to occur as the result of the decay of Langmuir waves located in regions where the angular gradient of the spectrum is maximum, i.e., around θ_c. This is because in this region the difference $N(k_1,\ \theta_1) - N(k_2,\ \theta_2)$ in equation (21) reaches its largest value. On the other hand, for the characteristic numbers of type III solar radio bursts being used in this analysis, our results (see Fig. 2) show that the ion-acoustic waves are preferentially directed toward angles around $\theta_S \sim 75^\circ$ (with respect to the direction of the decaying Langmuir wave). We can therefore expect that Langmuir waves with an angle θ_c with respect to the $\boldsymbol{e}_Z$-axis will preferentially produce ion-acoustic waves with an angle $\theta_S \sim 75^\circ - \theta_c$. This rough estimate gives peak angles of 70° and 50° for the two values of θ_c considered here, which is in agreement with the detailed numerical results shown in Figure 4.

In addition, in the perfectly collimated limit ($\theta_c \to 0$, $\Delta\theta \to 0$), from comparison with equation (13), we expect that peak values of P_1 will be close to 4, corresponding to the perfectly collimated case (see Fig. 2). The numerical results of Figure 4 are consistent with this. As a consistency check, Figure 5 shows the same results for a highly collimated distribution with $\theta_c = 0.^\circ 5$, $\Delta\theta = 0.^\circ 5$, and peak rates of $P_1 = 3.5$, at $\theta_S \sim 74^\circ$.

For a fixed $k_S = \langle k_L\rangle/10$, Figure 6 shows the effect of reducing the Langmuir wave distribution angular gradient. For a distribution with the edge centered at the angle $\theta_c = 5^\circ$, the left panel shows the resulting rates for $\Delta\theta = 2^\circ$ and 10°. The right panel shows the corresponding results for a distribution with the edge at the angle $\theta_c = 25^\circ$. The effect of a smoother distribution is to extend the possible angles of the produced ion-acoustic waves over a much wider range. In addition, as the angular gradient of the Langmuir spectrum is reduced, the difference $N_1 - N_2$ in equation (21) decreases, and hence $P_1(\theta_S)$ yields lower values.

Let us also compare the different diffusive decay rates against the corresponding backscattering decay rates. The backscattering of a Langmuir plasmon of wavenumber k_L produces an ion-acoustic plasmon of wavenumber $k_S = 2k_L - 2k_0$, as follows from taking the limit $\mu \to +1$ in equation (4). Figure 7 shows the resulting backscattering P_1 for the same two Langmuir spectra analyzed in Figure 4. Thin curves correspond to $k_S = 2k_{L,\,\min} - 2k_0$, and thick curves to $k_S = 2k_{L,\,\max} - 2k_0$. In this case, being the result of backscattering, the angular distribution of the decay rate closely follows that of the decaying Langmuir waves $N(k_1,\ \theta_1)$ in equation (21) (compare, e.g., Fig. 7, *right*, with Fig. 3).

A comparison between the backscattering results of Figure 7 and the diffusive decay results of Figure 4 shows that the diffusive rates are always larger, by factors of the order of 2–5. Figure 8 shows the same results for a highly collimated

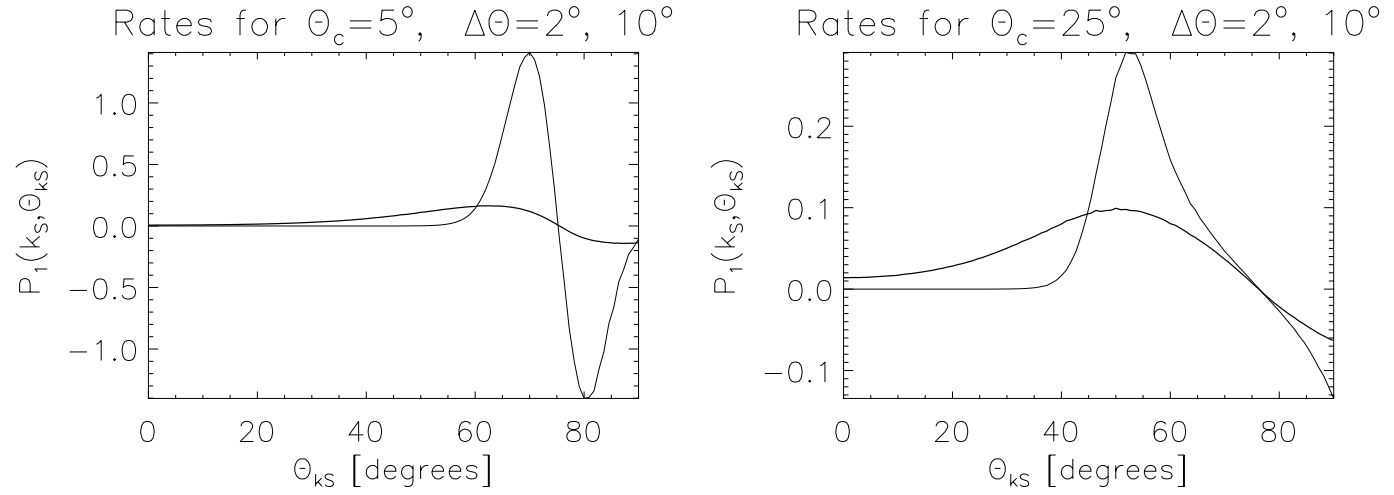

FIG. 6.—Dimensionless factor $P_1(k_s,\ \theta_S)$ for diffusive decay with a fixed $k_S = \langle k_L\rangle/10$, with $\theta_c = 5^\circ$ (*left*) and 25° (*right*), and $\Delta\theta = 2^\circ$ and 10° in both panels. Profiles are plotted as a function of θ_S, with the thin curve corresponding to $\Delta\theta = 2^\circ$ and the thick curve to $\Delta\theta = 10^\circ$.

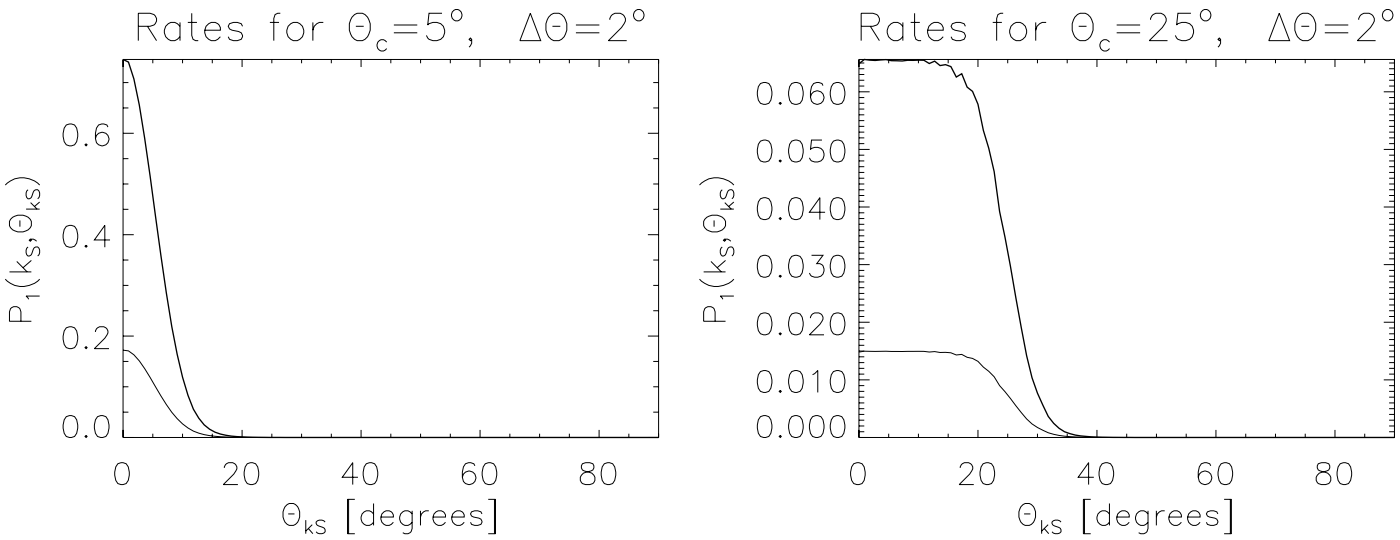

FIG. 7.—Dimensionless factor $P_1(k_s,\ \theta_S)$ for backscattering, with $\theta_c = 5^\circ$ (*left*) and 25° (*right*) and $\Delta\theta = 2^\circ$ in both panels. Profiles are plotted as a function of θ_S, with thin curves corresponding to $k_S = 2k_{L,\,\min} - 2k_0$ and thick curves to $k_S = 2k_{L,\,\max} - 2k_0$.

distribution with $\theta_c = 0\overset{\circ}{.}5$, $\Delta\theta = 0\overset{\circ}{.}5$. The resulting rates are of the order of $P_1 \sim 1.5$, or about a factor of 2 lower than the corresponding diffusive decay values of Figure 5. These results are consistent with the perfectly collimated beam results of Figure 2. Therefore, we find that, in all cases, diffusive decay rates are systematically larger than (although comparable to) the corresponding backscattering rates.

4. FREQUENCIES OF THE ION-ACOUSTIC WAVES

Several space-based missions, located at distances of the order of 1 AU from the Sun, are designed to perform in situ measurements of the extended solar wind. These missions are then able to perform in situ measurements of type III solar radio bursts, which sometimes extend far away from the Sun and reach the Earth. One of these instruments is URAP aboard the *Ulysses* mission. For the purpose of interpreting type III burst data collected by this experiment, let us suppose that an ion-acoustic wave travels through the region of the experiment. If $\boldsymbol{V}_{\rm sw}$ is the local solar wind velocity, the Doppler-shifted frequency of the ion-acoustic wave, as measured by the experiment, is given by

$$\begin{aligned} f_S &= \frac{1}{2\pi}\left(k_S V_S + \boldsymbol{k}_S \cdot \boldsymbol{V}_{\rm sw}\right) \\ &= \frac{k_S}{2\pi}\left[V_S + V_{\rm sw}\cos(\theta_{Sr})\right] \\ &= 2\frac{f_{\rm pe}}{V_\phi}\left[\cos(\theta_{SL}) - \frac{V_S V_\phi}{3V_{\rm Te}^2}\right]\left[V_S + V_{\rm sw}\cos(\theta_{Sr})\right], \end{aligned} \tag{23}$$

where k_S has been eliminated from equation (4), and θ_{SL} and θ_{Sr} are the angles between the propagation direction of the ion-acoustic wave and those of the primary (beam-aligned) Langmuir waves, and the (radial) solar wind, respectively. This formula is analogous to the one used by Cairns & Robinson (1995) to analyze a type III solar radio burst. They assume ES decay products only in the backscattering limit, and hence they consider the particular case $\cos(\theta_{SL}) = +1$. Also in that limit, the produced ion-acoustic waves propagate aligned with the beam direction, so that $\theta_{Sr} = \theta_{Lr}$, i.e., the angle between the primary Langmuir waves and the solar wind direction. On the other hand, in the diffusive limit, $\theta_{SL} > 0$ so that the angle θ_{Sr} takes the range of values $|\theta_{SL} - \theta_{Lr}| < \theta_{Sr} < \theta_{SL} + \theta_{Lr}$.

To quantify the predicted frequencies for the ion-acoustic waves in each of these two limiting cases, we refer to a specific observational case, analyzed by Thejappa & MacDowall (1998). They show the data of a type III solar radio event recorded by *Ulysses* URAP on 1995 March 14. Their detailed analysis shows radio emission at both the plasma and second harmonic frequencies. At the same time, impulsive ES fluctuations were recorded at the local plasma frequency, which turns out to be $f_{\rm pe} \sim 23$ kHz, identified as Langmuir wave bursts. The WFA (Wave Form Analyzer) instrument detected electric fluctuations, highly correlated in time with the observed Langmuir impulsive peaks, in the range 0–450 Hz. The instrument also detected magnetic field fluctuations in the range 0–50 Hz. The combination of these facts indicates that the electric field fluctuations in the range 50–450 Hz are of a pure ES nature, such as ion-acoustic waves. If this is the case,

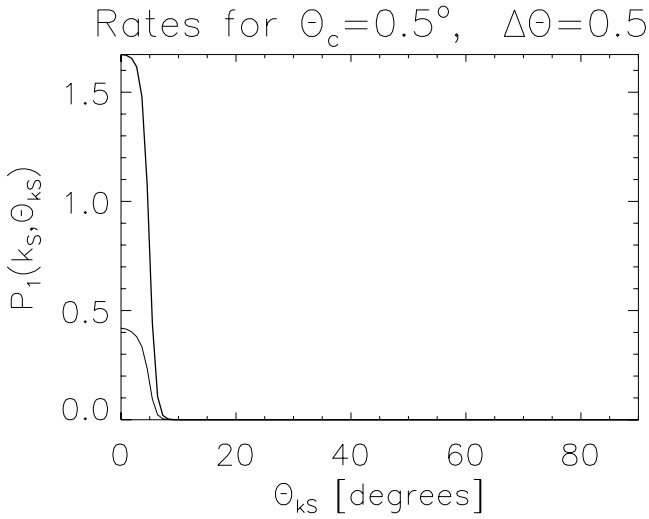

FIG. 8.—Dimensionless factor $P_1(k_s,\ \theta_S)$ for backscattering, with $\theta_c = 0\overset{\circ}{.}5$ and $\Delta\theta = 0\overset{\circ}{.}5$. Profiles are plotted as a function of θ_S, with the thin curve corresponding to $k_S = 2k_{L,\,\min} - 2k_0$ and the thick curve to $k_S = 2k_{L,\,\max} - 2k_0$.

their strong temporal correlation with the Langmuir bursts supports the idea that the ion-acoustic waves may be produced by the ES decay of the L waves (see also Cairns & Robinson 1995). On the other hand, fluctuations below 50 Hz are most likely of electromagnetic nature, such as whistlers. In summary, the analysis by Thejappa & MacDowall (1998) strongly suggests the presence of ion-acoustic waves in the range 50–450 Hz, for this particular event, and that these waves are produced as the result of the ES decay of beam-excited Langmuir waves.

For the event under consideration, the numerical values of the relevant parameters are (Thejappa & MacDowall 1998): $V_S = 5.1 \times 10^6$ cm s^{-1}, $V_{\rm Te} = 1.6 \times 10^8$ cm s^{-1} (corresponding to $T_e = 1.7 \times 10^5$ K), $V_{\rm sw} = 3.4 \times 10^7$ cm s^{-1}, $V_\phi \sim V_{\rm beam} \pm 25\%$, with a mean beam velocity estimated to be $V_{\rm beam} = 3.5 \times 10^9$ cm s^{-1}, $f_{\rm pe} = 2.3 \times 10^4$ Hz, and $\theta_{Lr} \sim 45^\circ$.

Using these numerical values, we now compute, in the two limit cases under analysis, the predicted ion-acoustic wave frequencies. In all cases, we assume that the primary (beam-excited) Langmuir waves form a mean angle $\theta_{Lr} = 45^\circ$ with respect to the solar wind direction and that the primary Langmuir waves have phase speeds in the range $V_\phi = V_{\rm beam} \pm 25\%$.

Figure 2 shows that, in the diffusive limit, decays most likely proceed for angles θ_{SL} in the range 60°–75° (in this range, the probability is about twice the backscattering probability). Using this range of angles in equation (23), we find that the diffusive-scattering assumption yields ion-acoustic waves in the range 50–215 Hz. On the other hand, if backscattering is assumed, we have $\theta_{SL} = 0^\circ$, and equation (23) yields ion-acoustic frequencies in the range 215–415 Hz. The difference between the predictions in both limits is due to the term $[\cos\theta_{SL} - (V_S V_\phi / 3V_{\rm Te}^2)]$, which is maximized in the backscattering case as $\cos(\theta_{SL}) \sim +1$.

If the primary Langmuir waves form a variable angle $0^\circ < \theta_{Lr} < 90^\circ$ with respect to the solar wind direction, the frequency ranges predicted in both limits overlap each other, within the observed range. In this case, the backscattering limit yields predicted ion-acoustic frequencies over the whole observed range (as already pointed out by Thejappa & MacDowall 1998). We thus find that the predictions for both asymptotic cases are consistent with the observations. Taking mean values of the different parameters, we find out that for the backscattering assumption, the predicted frequencies are consistent with the higher frequency portion of the observations (see also Cairns & Robinson 1995). On the other hand, the diffusive-scattering limit yields predicted frequencies that are consistent with the lower frequency portion of the observed ES fluctuations.

Further empirical support arises from recent observational work by Thejappa et al. (2003), in which they analyze URAP data for another type III burst, in a fashion similar to the case already described. This case corresponds to in situ observations at much larger heliocentric distances, specifically at 5.2 AU, where the local ambient plasma parameters are very different ($f_{\rm pe} \sim 2$ kHz, $T_e \sim 8.8 \times 10^4$ K) from those of the previous case. The beam velocity (and hence the primary Langmuir wave phase velocity) is estimated to be $V_\phi \sim 1.5 \times 10^9$ cm s^{-1} $\pm$ 30%. In this other case, the URAP WFA also detected electric field fluctuations correlated in time with Langmuir bursts. The electric waves that can be safely assumed to be of ES nature (i.e., with no simultaneous detection of magnetic field fluctuations above the background level) are in the frequency range 20–200 Hz.

We repeated our probability calculations for this case and found that, in the diffusive limit, decays proceed most likely for angles θ_{SL} in the range 55°–73° (in this range the probability is about twice the backscattering probability). Using this range of angles, in the diffusive limit the predicted ion-acoustic frequencies are in the range 0–60 Hz. On the other hand, under the backscattering assumption the predicted frequencies are in the range 55–105 Hz.

5. CONCLUSIONS

From the theoretical point of view, an analysis of the ES decay rate indicates that the process is dominated by two limiting cases: diffusive (small-angle) scattering and backscattering. We find that the decay rates are comparable for both cases, with the diffusive decay rates being systematically larger than those in the backscattering limit. Given the results of our quantitative comparative analysis, we believe that both limiting cases are acting at the same time. Furthermore, we speculate that the net effect of diffusive decay and backscattering acting simultaneously is then that of a diffusive isotropization of the beam-generated Langmuir spectrum. The backscattering generates a backward-directed spectrum (with respect to the beam propagation direction), but then this secondary spectrum can also diffuse by small-angle decay. Thus, if ES decay is assumed to be present in solar flare and type III solar radio burst scenarios, we believe that its ability to isotropize Langmuir waves cannot be neglected.

From an observational point of view, we refer to the analyses of type III bursts by Thejappa & MacDowall (1998) and Thejappa et al. (2003). They registered low-frequency ES fluctuations that are strongly correlated in time with impulsive Langmuir wave bursts. We find that the observed frequencies of these fluctuations are consistent with the predicted frequencies of ion-acoustic waves produced by the ES decay of the primary (beam-excited) Langmuir waves. Under the backscattering assumption, the predicted frequencies are consistent with the higher frequency portion of the observations. On the other hand, the diffusive-scattering limit yields predicted frequencies that are consistent with the lower frequency portion of the observed ES fluctuations. The relative burst intensities in the two frequency ranges could then serve as a proxy for the relative effectiveness of the ES decay in each limit, which we anticipate to be comparable from our theoretical analysis.

From this analysis, we speculate that both the backscattering and diffusive limits of the ES decay may be relevant in type III bursts (and presumably also in solar flare radio events). In addition, the beam-generated Langmuir turbulence may become isotropic as the ES decay proceeds, mainly in the two limiting cases of diffusive scattering and backscattering. We postpone for a future work the investigation of the coupling between the ES decay and the quasi-linear beam-turbulence interaction. We believe that the simultaneous consideration of both effects can bring HXR and radio emission predictions into a better agreement with observations. This is due to the fact that inclusion of the coupling will imply a limitation of the effectiveness of the quasi-linear relaxation, yielding lower Langmuir turbulence levels, and hence lower radio emissivity.

We thank the anonymous referee for useful suggestions that helped to clarify our main conclusions. This work was funded

by the Agencia Nacional de Promoción de Ciencia y Tecnología (ANPCyT, Argentina) through grant 03-09483. We also thank Fundación Antorchas (Argentina) for partial support through grant 14056-20.

REFERENCES

Cairns, I. H. 1987, J. Plasma Phys., 38, 179
Cairns, I. H., & Robinson, P. A. 1995, ApJ, 453, 959
Edney, S. D., & Robinson, P. A. 2001, Phys. Plasmas, 8, 428
Emslie, A. G., & Smith, D. F. 1984, ApJ, 279, 882
Hamilton, R. J., & Petrosian, V. 1987, ApJ, 321, 721
Melrose, D. B. 1982, Sol. Phys., 79, 173
Thejappa, G., & MacDowall, R. J. 1998, ApJ, 498, 465
Thejappa, G., MacDowall, R. J., Scime, E. E., & Littleton, J. E. 2003, J. Geophys. Res., 108, SSH 9-1
Tsytovich, V. N. 1970, Nonlinear Effects in Plasma (New York: Plenum)
Vásquez, A. M., & Gómez, D. O. 1997, ApJ, 484, 463
Vásquez, A. M., Gómez, D. O., & Ferro Fontán, C. 2002, ApJ, 564, 1035